Nanometer Positional Control using Magnetic Suspension for Vacuum-to-Air Mass Metrology

Nicholas Vlajic
Mechanical Engineer, ASME Member
National Institute of
Standards and Technology
Gaithersburg, MD, USA
Email: Nicholas.Vlajic@nist.gov

Melissa Davis
Joint Quantum Institute Student
National Institute of
Standards and Technology
Gaithersburg, MD, USA

Corey Stambaugh*
Physicist
National Institute of
Standards and Technology
Gaithersburg, MD, USA
Email: Corey.Stambaugh@nist.gov

This paper explains the control scheme that is to be used in the Magnetic Suspension Mass Comparator (MSMC), an instrument designed to directly compare mass artifacts in air to those in vacuum, at the United States National Institute of Standards and Technology. More specifically, the control system is used to apply a magnetic force between two chambers to magnetically suspend mass artifacts, which allows for a direct comparison (i.e., a calibration) between the mass held in air and a mass held in vacuum. Previous control efforts that have been demonstrated on a proof-of-concept of this system utilized PID-based control with measurements of the magnetic field as the control signal. Here, we implement state-feedback control using a laser interferometric displacement measurement with a noise floor of approximately 5 nm (root-mean-square). One of the unique features and main challenges in this system is that, in order to achieve the necessary accuracy (relative uncertainty of 20×10^{-9} *in the MSMC), the magnetic suspension must not impose appreciable lateral forces or moments. Therefore, in this design, a single magnetic actuator is used to generate a suspension force in the vertical direction, while gravity and the symmetry of the magnetic field provide the lateral restoring forces. The combined optical measurement and state-feedback control strategy presented here demonstrate an improvement over the previously reported results with magnetic field measurements and a PID-based control scheme.*

*Address all correspondence to this author.

1 Introduction

Mass metrology relies on an unbroken chain of comparisons between mass artifacts to establish traceability and standardization of mass to the International System of Units (SI) definition of mass, namely the International Prototype of the Kilogram [1]. Among the many challenges in precision mass metrology are environmental effects, which play a large role in correcting for buoyancy and sorption – *sorption* is the general process by which contaminant molecules are retained on (*adsorption*) or leave (*desorption*) the surface of a solid body [2, 3]. The buoyancy correction is dependent on the volume of the artifact and the density of air, which in turn is dependent on the pressure, humidity, and temperature of the environment [1, 4]. Accounting for these effects becomes even more important when comparing mass artifacts of nominally the same mass, but of different volumes and densities, as the buoyancy force is dependent upon the volume difference, and the sorption effects are proportional to the surface areas. An even more critical need to address environmental effects will occur in the redefined SI, wherein the new definition of the kilogram is defined in vacuum and an artifact will be used to transfer the definition to other artifacts in air [5, 6].

Although buoyancy corrections can generally be well determined, mass corrections originating from sorption effects is still empirical and can vary in different experiments [7, 8]. The current method for determining sorption is through sorption-artifact studies. These measurements compare mass artifacts of similar mass and volume but differing surface area to determine an *expected* mass change per unit area due to adsorption/desorption. This expected mass change is then applied to the calibration of *other* mass arti-

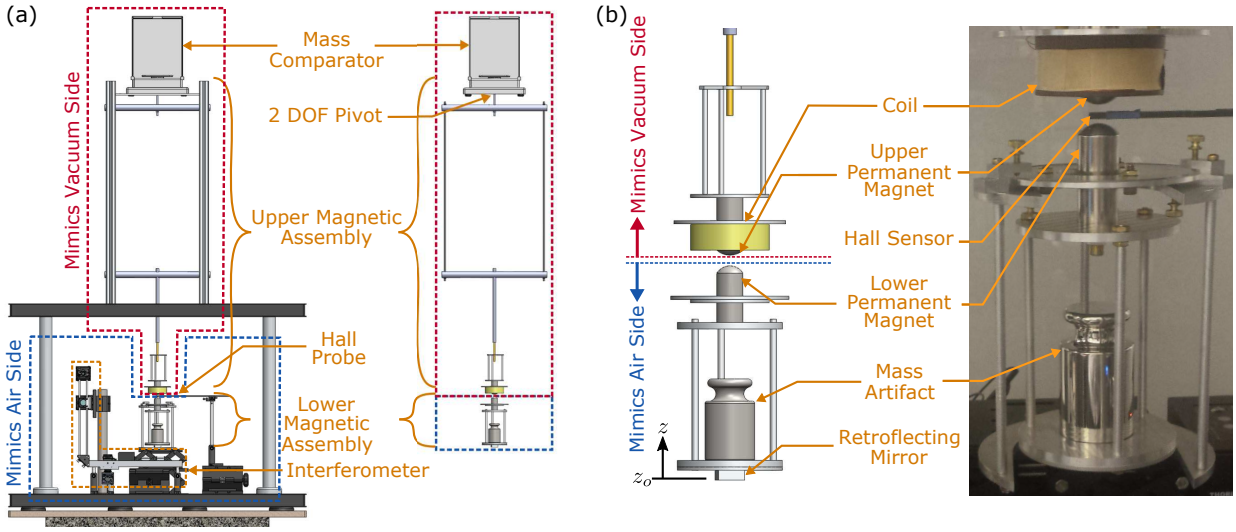

Fig. 1. Components of the Proof-of-Concept (POC) system: (a) Digital rendering of the system with annotated components and (b) photograph of the lower weigh pan and 1 kg mass, collectively referred to as the Lower Magnetic Assembly (LMA). The LMA is fully suspended using magnetic levitation in this photograph.

facts when one artifact is held in vacuum and the other in air. This approach has its drawbacks. First, the expected mass change is dependent upon the environmental conditions during the sequence of measurements as well as the material and material properties of the artifacts. Furthermore, it is an *indirect* method in the sense that sorption correction is determined from one artifact (the sorption-artifact pair) and applied to another (the mass artifact to be calibrated). In effect, one is creating transfer standards between air and vacuum and relying on their stability. Another significant drawback to this method is the extensive amount of time needed to make a single sorption measurement, as it takes days to weeks for the mass artifacts to stabilize in vacuum and again when transferred into air [9].

An alternative approach, pioneered at the National Institute of Standards and Technology (Gaithersburg, Maryland, USA), relies on making a direct comparison between a mass artifact in air and an artifact held in vacuum, where a link to the comparison is established by magnetically suspending one of the artifacts [10, 11]. The prime advantage of this system is that it is a *direct* method in the sense that the vacuum mass calibration is transferred directly to the mass in air without the need of a sorption-artifact transfer standard. Furthermore, a single measurement sequence can be taken in tens of minutes, rather than days, allowing for several measurements which can be averaged to reduce the statistical uncertainty. Moreover, this method is independent of the artifacts' surface properties. This system is referred to as the Magnetic Suspension Mass Comparator (MSMC) [12]. A more detailed description of this system is given in Section 2.

We note that use of magnetic suspension to facilitate the measurement of force or a related unit (e.g., mass or density) of a quantity under different environmental conditions is not unique to our apparatus [13]. Measurements of thermodynamic equations of states and fluid densities using densimeter instruments have been performed for decades [14–16]; however, there are fundamental differences – and likewise challenges – between these systems and the MSMC. In density measurements, an electromagnetic actuator, which is attached to a mass comparator, is used to suspend a mass artifact (or artifacts) in an enclosed chamber that can be filled with fluids under varying environmental conditions (e.g., temperature and pressure). The density of the fluid is calculated by measuring the change in the buoyant force of the same mass artifact (or artifacts) [17, 18]. In contrast, in the MSMC the mass difference between two *artifacts* located in two separate environments using the same mass comparator is measured; thus, the vacuum artifact is never in air, and the air artifact is never in vacuum. This fundamental difference eliminates the application of the approaches and techniques used in the aforementioned densimeters to the MSMC [18]. It is noteworthy to mention that MSMC must suspend a much larger value of mass (by as much as 30 times in comparison to densimeters), and the desired level of precision is also higher, since it is used for dissemination of the primary standard at 1 kg [1].

It is instructive to discuss the operation of a mass comparison for traditional mass calibrations, as it serves to illustrate the operation of the MSMC. Specifically, the goal is to determine the mass value of an unknown artifact by comparing it to the mass value of a known artifact. Traditional calibrations, using a single-pan apparatus, are performed as follows [1,19]. An instrument, referred to as a mass-comparator or mass-balance, is used as an indicating instrument where the indication (a digital or analog recording) from the instrument is proportional to the force on its weighing pan – mass is then determined by accurately correcting for local gravity and making the necessary environmental corrections. First, the known mass is placed on the weigh pan and a reading is recorded. Subsequently, the known mass is removed from the pan and the unknown mass is placed on the weigh pan. Using the value of the known mass and the difference

in the indication, the value of the unknown mass can be determined [1] [1]. We note that in practice, modified versions of this process, which employ multiple masses and multiple readings for averaging, are often used to reduce the uncertainty in the calibration [1].

In the MSMC, this same process is utilized; however, there are two weighing pans, as opposed to a single weighing pan. One weighing pan is connected to the comparator via mechanical linkage and is kept in a vacuum chamber along with at least one mass artifact. The second pan (and corresponding mass) is kept in a separate chamber containing air. The two weighing pans are coupled through an actively controlled magnetic suspension force. The focus of this paper is the measurement and control scheme used to magnetically suspend the weigh pan and mass in air. The robustness and stability of the control scheme is critical in achieving accurate mass measurements with minimal standard deviations.

Magnetic suspension for precision mass metrology has been used prior to the 1950's with the work of Clark [20]. Notable contributions with regard to mass metrology were also made in the 1950's by Beams [13, 21]. Furthermore, active feedback for positioning to nanometer precision outside of the context of mass metrology has been demonstrated in several separate efforts, including those by Refs. [22–24] to name a few. The MSMC system differs from these systems, and likewise poses other engineering and controls challenges. First, we are not using the controller output (i.e., voltage or current) to determine mass as was done in Refs. [13, 21]; rather we are using the controller as an effective link across the wall of two chambers. Furthermore, our magnetic solenoid used for suspension is not fixed in space; rather it is secured to the end of a pendulum that is free to swing and move laterally about a pivot, which presents limitations regarding the extent to which the position of the levitating mass can be controlled. This degree-of-freedom pivoting motion is essential to the design of the balance, as the weigh pans must be free to swing and align with gravity and any lateral constraints will impose cosine-type errors. The previous works of Refs. [22–24] used multiple actuators and sensors to achieve their desired accuracy. We demonstrate positional control to less than 75 nm standard deviation using only a single actuator.

The remaining portions of this paper are as follows. In Section 2, the MSMC and its relation to the proof-of-concept system POC is explained. Following in Section 3, a reduced-order model that was originally presented in Ref. [25] is described, as well as the control scheme that is used to suspend one of the mass artifacts. A validation of the modeling by comparisons with simulation results and experimental data is presented in Section 4. Within this section, comments are given on the use of this controller for suspension for mass metrology. Finally, a summary and concluding remarks are presented in Section 5.

[1] Additional step(s) are required to calibrate the comparator or balance, as the indication from the instrument must be converted to units of mass.

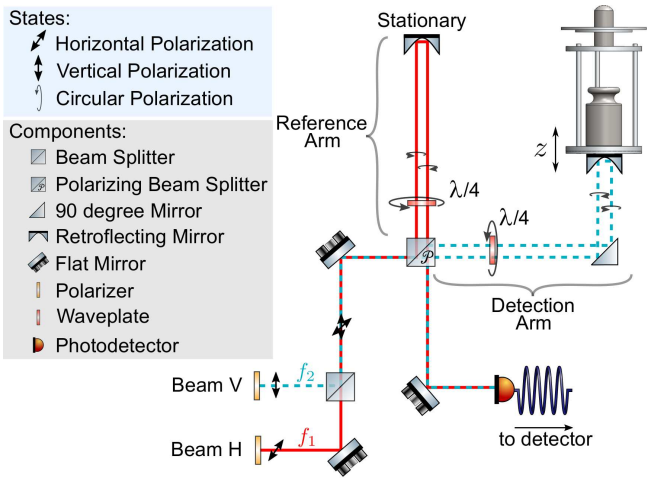

Fig. 2. Optical interferometer used to measure displacement of the suspended mass.

2 Description and Operation of the MSMC and POC Systems

2.1 System Description and Operation

A schematic of the proof-of-concept (POC) system, which has been constructed to mimic the MSMC, is shown in Fig. 1. The MSMC is composed primarily of a mass comparator with two weighing pans. One pan is directly connected to the comparator which sits in a vacuum chamber, while the other pan is magnetically suspended from below the comparator in a chamber that contains air. It is worth noting that in the POC system, both weighing pans and masses are in air, but in the MSMC, the mass-comparator and weighing pan are in vacuum. The ability to weigh a mass with a magnetic link to the lower weighing pan is the prime feature of the MSMC which allows for the vacuum-to-air dissemination. This direct connection allows for readings to be made of samples under extremely different environments than the mass comparator [8]. This method also has the advantage that the measurements can be made within minutes, rather than days or weeks. We refer to the suspended portion of the system, including the lower weigh pan, as the lower magnetic assembly (LMA), and the portion including the mass-comparator, upper weigh pan, and linkage as the upper magnetic assembly (UMA).

The bulk of the lifting force for the magnetic suspension is realized by two permanent rare-earth magnets. One is connected to the UMA, while the other to the LMA. An electromagnetic coil is wrapped around the magnet in the UMA, which used in conjunction with the control system, provides the time-varying force necessary to keep the LMA suspended in air. To monitor the position of the suspended LMA, both a magnetic sensor (based on the Hall effect) and an interferometric displacement measurement are implemented. Previous control schemes used the magnetic field as the measured signal for control [25]. Within this work, the control measurement is done using the displacement from the interferometer, along with a different control scheme based on state-feedback.

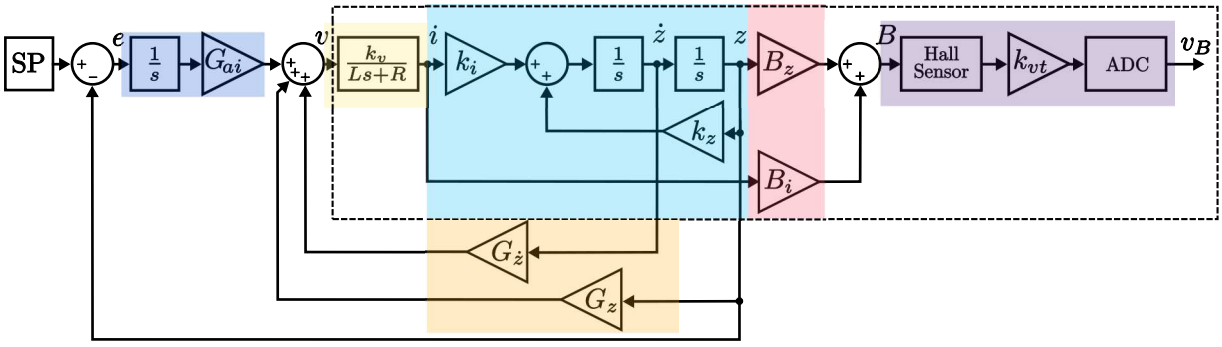

Fig. 3. Block diagrams for state feedback control. Yellow: Magnetic coil. Blue: Mechanics of the LMA. Red: B-field. Purple: B-field measurement. Dark blue: Action integrator. Orange: State feedback.

A schematic of the interferometer system used to measure the displacement of the magnetically suspended mass is shown in Fig. 2. The interferometer is based on the heterodyne principle, wherein the beam is composed of two orthogonally polarized beams which differ in frequency by nominally 3 MHz. The beams are split by sending the light through a polarizing beam splitter. Thereafter, one of the polarized beams of frequency f_1 strikes a stationary reference retroflecting mirror, while the beam of the second polarization and frequency $f_2 = f_1 + 3$ MHz strikes the retroflecting mirror secured to the base of the LMA weigh pan. The beams are then recombined and interfered at the photodetector. By measuring deviations in the nominal difference frequency between the two beams, the velocity and position of the observed object, here the bottom of the LMA, can be determined. It is noted that this interferometric measurement is fundamentally a determination of the difference in the path length between the two beams and not strictly a measure of the vertical displacement z. Consequently, small lateral and angular motions of the LMA will result in a change in the effective path length and show up as errors in z. These effects can be mitigated by replacing the retroflecting mirrors with flat mirrors; however, the measurement system becomes sensitive to angular motions and significant challenges arise in aligning the beams so that they interfere to create a meaningful signal. The spectral noise floor of the interferometer (without suspension) is around 2 nm between 0 Hz - 1 Hz (10 second integration time), below 1 nm for frequencies above 1 Hz (10 second integration time).

3 Reduced-Order Model and Control of the POC System

3.1 System Model and Dynamics

Mass comparisons in the MSMC are only operated when the magnetic suspension is actively controlled, but it is worth discussing the open-loop dynamics. A graphic of the open-loop block diagram is shown within the dashed box of Fig. 3. The development of the governing equations of motion in the Laplace domain is given in Ref. [25], but we restate them here in time domain for completeness. Note that we neglect the dynamics of the Hall sensor (effectively a 5 kHz low-pass filter) and the ADC (effectively a tunable 300 Hz low-pass filter) because their dynamics are much faster than that of the rest of the system, and their gains are relatively constant in the operating frequency range of interest. The governing equations of motion are written:

$$\dot{i} = -\frac{R}{L}i + \frac{k_v}{L}v \text{ and} \tag{1}$$

$$\begin{aligned} m\ddot{z} &= f_m(z,i) - mg \\ &= f_{mi}(i) + f_{mz}(z) - mg. \end{aligned} \tag{2}$$

In Eqn. (1), i is the current through the electromagnetic coil, while R and L are the lumped-parameter resistance and inductance of the coil, respectively. The quantity k_v is a gain that amplifies the controller output voltage to the applied voltage across the coil.In Eqn. (2), m is the mass of the lower magnetic assembly and g is the local acceleration due to Earth's gravity. The total magnetic force $f_m(z,i)$ is a superposition of the magnetic force from the drive current $f_{mi} \equiv f_{mi}(i)$ and magnetic force from the position of the magnet $f_{mz} \equiv f_{mz}(z)$, and v is the control voltage with amplifier gain k_v. The magnetic force from the current $f_{mi}(i)$ is an experimentally determined and polynomial-fit as a function of i, while the magnetic field as a function of position $f_{mz}(z)$ is experimentally measured and least polynomial-fit in z. The upper and lower magnets are of opposite polarity, and the set point z_o is determined from the fixed points of Eqns. (1) and (2), which corresponds to $i = 0$ and $z_o = f_{mz}^{-1}(mg)$, where superscript -1 denotes the functional inverse. The two functions are then linearized about this point and are written:

$$f_{mi}(i) \approx \bar{k}_i i \tag{3}$$

$$f_{mz}(z_o + z) \approx mg + \bar{k}_z z, \tag{4}$$

where $\bar{k}_z, \bar{k}_i > 0$ are constants. For z_o used here, the linear approximation is good to within 1 % over a displacement of $\pm 100\,\mu$m. It is clear from the structure of Eqns. (1)-(4), that the fixed point is an unstable node with eigenvalues $\lambda_{1,2,3} = \{\sqrt{\bar{k}_z/m}, -\sqrt{\bar{k}_z/m}, -R/L\}$. For notational convenience, we introduce $k_i = \bar{k}_i/m$ and $k_z = \bar{k}_z/m$, and write the linearized

form of Eqn. (2) as

$$\ddot{z} = k_i i + k_z z \tag{5}$$

3.2 Position Closed-loop State Feedback Control

The control scheme that is used to magnetically suspend the LMA is described within this section. The objectives of the controller are to (1) decrease the settling time (to minimize the time between mass readings) and (2) be robust to disturbances around the operating point so that the standard deviation around the operating point is minimized.

As mentioned earlier, in the current state of the POC system, a laser interferometer is used to measure the displacement of the suspending weighing pan. This displacement measurement allows for state-feedback to be implemented on the z coordinate and on an estimate of $\dot{z}$. This is in contrast to using the B-field measurement and a state estimator for the entire system. An action integral with gain G_{ai} has been included to ensure the displacement value goes to the set point, since in practice, the set point and final value may have small differences because of errors in the identified system parameters. Introducing the error $e = z_o - z$, we write the system state vector as $x = \{i, z, \dot{z}, e_i\}^\mathsf{T}$, where the super-script T denotes the matrix-vector transpose and $e_i = \int_0^t e(\tau)\, d\tau$. The system can then be written as

$$\dot{x} = Ax + Bu \tag{6}$$

$$y = Cx + Du \tag{7}$$

where

$$A = \begin{bmatrix} -\frac{R}{L} & 0 & 0 & 0 \\ 0 & 0 & 1 & 0 \\ k_i & k_z & 0 & 0 \\ 0 & 1 & 0 & 0 \end{bmatrix}, \; B = \begin{bmatrix} \frac{K_v}{L} \\ 0 \\ 0 \\ 0 \end{bmatrix}, \tag{8}$$

$$C = \begin{bmatrix} 0 & 1 & 0 & 0 \end{bmatrix}, D = 0. \tag{9}$$

The control signal, denoted u, is constructed from feedback with an action integral, as

$$u = -\left(G_z z + G_{\dot{z}} \dot{z} + G_{ai} e_i\right), \tag{10}$$

where G_z is an effective stiffness gain, $G_{\dot{z}}$ is an effective damping gain, G_{ai} is the gain of the action integral, and $\dot{z}$ is estimated by numerical differentiation followed by low-pass filtering. With state-feedback, the stability of the controlled system can be determined by examining the eigenvalues of the matrix

$$\hat{A} = \begin{bmatrix} -\frac{R}{L} & -\frac{G_z k_v}{L} & -\frac{G_{\dot{z}} k_v}{L} & -\frac{G_{ai} k_v}{L} \\ 0 & 0 & 1 & 0 \\ k_i & k_z & 0 & 0 \\ 0 & 1 & 0 & 0 \end{bmatrix}, \tag{11}$$

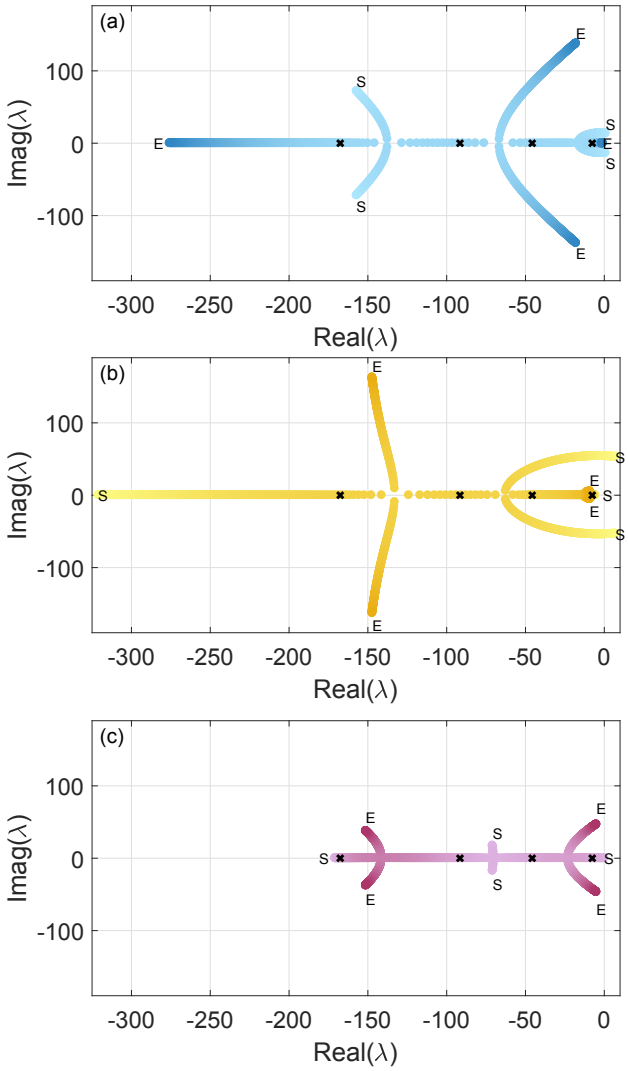

Fig. 4. Eigenvalues λ of the state-feedback control system, while varying gain parameters (a) G_z, (b) $G_{\dot{z}}$, and (c) G_{ai}. Lighter shades of color represent small gain values (also denoted by the letter "S" for "starting"), while darker color shading represents larger gain values (also denoted by the letter "E" for "ending"). The black × mark indicates the eigenvalues used in normal operation of the system. Part (a): Varying $G_z \in \{10^2, 10^5\}$ (corresponding to colors {●,●}) while $G_{\dot{z}} = 550$ and $G_{ai} = 10^5$. Part (b): Varying $G_{\dot{z}} \in \{0, 10^3\}$ (corresponding to colors {●,●}) while $G_z = 17 \times 10^3$ and $G_{ai} = 10^5$. Part (c): Varying $G_{ai} = \in \{0, 10^6\}$ (corresponding to colors {●,●}) while $G_z = 17 \times 10^3$ and $G_{\dot{z}} = 550$.

which can be found by substituting Eqn. (10) into Eqn. (6) along with Eqn. (8).

The eigenvalues of Eqn. (11) are plotted in Fig. 4 as a function of the gain parameters $\{G_z, G_{\dot{z}}, G_{ai}\}$. Lighter shades correspond to low values of gain parameters, while darker shades correspond to higher values of gain. The black × marks in Fig. 4 denote the eigenvalues of the system when used in operation. While keeping $G_{\dot{z}}$ and G_{ai} fixed, the system is unstable (corresponding to real(λ) > 0) for small G_z, but as G_z increases, the system becomes stable (corresponding to real(λ) < 0). Similarly, when $G_{\dot{z}}$ is zero, the system is

unstable, but becomes stable as it is increased. The system is always stable over the range of G_{ai} that was tested, but the system will become unstable for larger values of G_{ai}.

There is a trade-off between the two controller objectives, namely quick response time and robustness to disturbances around the operating point. Larger values of G_z will make the system respond faster (a larger negative eigenvalue); however, large G_z values will amplify noise in the measurement which will lead to motions around the set point and ultimately a larger standard deviation in the mass readings. The action integrator term G_{ai} will help smooth some of the deviations around the set-point, but the system will not respond as quickly.

4 Experimental Measurements and Comparison with Simulations

4.1 Measurement and Simulation Comparison

A comparison between the simulation and the model given a 20 μm step input is shown in Fig. 5(a). The simulations were performed using the values shown in Tab. 1 in MATLAB and Simulink [2] [26].

The mass reading deviations from the nominal value (approximately 4.182 kg) are also provided in Fig. 5(b). Good agreement between the simulation and experiment using PID control was already presented in the detailed model given in Ref. [25]. The sample rate of the mass balance is approximately 10 Hz (limited by the manufacturer's software), while the displacement measurement was 5 kHz. There is also a delay between the mass readings and the interferometer measurement. In practice, these comparators are used to make static mass measurements, and the output signal is typically filtered internally by software on the balance. We note that for the mass readings presented within this work, the filtering has been disabled on the comparator instrument with the intent of being able to benchmark the performance with gain parameters without any influences from the comparator digital filters.

Good agreement is observed between the experiment and simulation using state feedback control. With the gain parameters selected here, the mass quickly jumps to the set point with little overshoot. There are small oscillations in the response that are observed in the experiment, but not predicted by the simulation. These oscillations are likely due to rocking or tilting motions of the mass and the mathematical model does not account for these types of motion. The faster response and settling-time of the system presented here is a notable improvement from the response shown in Ref. [25]. The response shown in Fig. 5(a) is also consistent with the system eigenvalues shown in Fig. 4 (denoted by black × marks), as they are eigenvalues with negative real-part and no imaginary parts, which would correspond to a stable response without any oscillations.

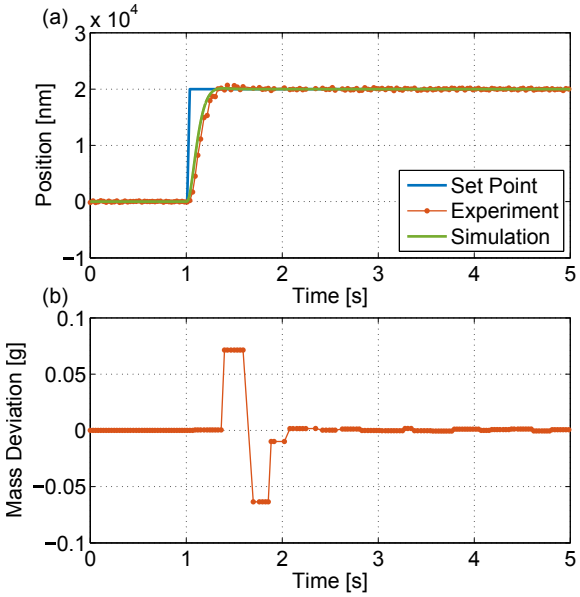

Fig. 5. (a) Comparison between experiments and simulations and (b) mass deviations from nominal value during the step.

Table 1. Identified parameters of the proof-of-concept (POC) system used in the simulations.

Quantity	Value	Unit
k_v	4.2	V
k_{vt}	5.0	V/T
R	40	Ohm
L	0.144	H
k_i	1.85	N/(A · kg)
k_z	980	N/(m · kg)
B_z	40	T/m
B_i	0.024	T/A
G_{ai}	1×10^5	V/(m · s)
G_z	17×10^3	V/m
$G_{\dot{z}}$	550	(V · s)/m

4.2 Performance of Controller for Vacuum-to-Air Dissemination

Measurements on the deviations of the motion from the set-point and the corresponding mass-value as a function of frequency are presented in Fig. 6(a) & (b), respectively. For comparison purposes, the noise floor of the displacement and mass reading are also shown. In all the measurements shown in Fig. 6, the data were obtained by 20 averages of 10 seconds of data. Not surprisingly, the amplitude of the displacement increases by factors of 10 to 100 in the case with suspension to without suspension. In the time domain, the standard deviation increases from roughly 5 nm to 75 nm; however, we consider this a worst-case scenario since the LMA and mass did not have tightly controlled environmental con-

[2] Certain commercial equipment, instruments, or materials are identified in this article in order to describe the experimental procedure adequately. Such identification is not intended to imply recommendation or endorsement by the National Institute of Standards and Technology, nor is it intended to imply that the materials or equipment identified are necessarily the best available for the purpose.

ditions. It is worth mentioning that we have achieved stabilization with standard deviations lower than 40 nm for durations of tens of seconds, although results are not shown. As noted earlier, the displacement measurement is fundamentally a measure of the relative distances between the stationary mirror and the mirror mounted to the LMA, such that lateral and tilting motions of the LMA will also show up at displacement measurements. When this controller and interferometer are implemented in the MSMC, although still in air, the LMA and corresponding mass will be better shielded from air currents and the deviations from the set-point are expected to be lower. The two spikes in the spectra around the set-point at 0.5 Hz and 1.7 Hz likely correspond to pendulum motions of the assembly, while the large, broad peak at 65 Hz in the unsuspended spectra results from motion of the support frame used to hold the retro-reflector.

Although the deviations of the displacement from the set-point increase from the case with no suspension (i.e., the noise floor) to the case with suspension, the deviations of the mass reading from nominal are unaffected at lower frequencies. Note that slow drifts, likely originating from changes in air pressure in the room, have been subtracted from the data; remaining variations at the lowest frequency can be attributed to residual drifts. In the MSMC system, the air chamber will be tightly sealed and the pressure will be monitored inside to make these corrections. Furthermore, as mentioned earlier, the mass-balance is giving unfiltered mass values. Once the mass filtering is reinstated, the standard deviations at higher frequencies will be attenuated. The data in Fig. 6 suggest that the resolution of the balance is the limiting factor in the mass determination and not the control or measurement scheme. It is worth pointing out that the deviations in mass shown in Ref. [25] were filtered; thus, while noise levels between the two look similar, this current scheme is an improvement as it will attenuate higher frequencies excitation even further once the filtering is reinstated.

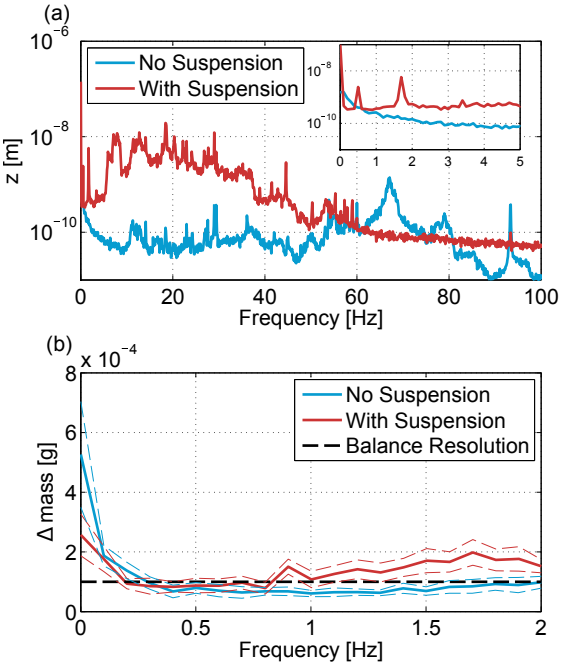

Fig. 6. (a) Displacement noise floor with 20 averages of 10 seconds of data with and without suspension. (b) Mass noise floor with 20 averages of 10 seconds of data with and without suspension. The dashed lines represent the ($k = 2$) standard deviation of the mean.

5 Concluding Remarks on Implementation in the MSMC

The control scheme, analysis, and measurements presented here were demonstrated on a proof-of-concept system. Ultimately, this measurement and control system will be implemented in the NIST Magnetic Suspension Mass Comparator for vacuum-to-air mass dissemination. One of the unique features and challenges of this system is that only one actuator is used to control the vertical position, while the remaining lateral degrees-of-freedom are restored by gravity and radial symmetry of the magnetic field. Deviations of the displacement around the set-point where measured to be less than 100 nm standard deviation, which includes vertical and lateral displacements; however, the standard deviation of the mass readings was not affected during suspension and the limitation of the mass-value was governed by the resolution of the balance. The resolution of the balance in the POC is 100 μg, while in the balance in the MSMC is 10 μg. This suggests that mass readings with even lower standard deviations can be achieved in the MSMC once the control and measurement system have been implemented. Furthermore, the displacement deviations are anticipated to be smaller in the MSMC since the environment in which the artifact and LMA are kept will be better controlled and air currents will be minimized.

Finally, the data presented in Section 4.2 indicate that the controller is not the limiting factor in the statistical uncertainty of the mass measurements; however, several other uncertainty contributions must be considered when this controller is implemented in the MSMC system. For instance, corrections due to buoyancy effects and gravity must be characterized [6]. More critical, interactions of the two magnets with the outside environment must be measured. Work has already been done to measure the spatial distribution of the field outside the magnets [12]. In order to characterize the influence of these external magnetic field interactions on the mass values, the noise floor of the mass readings (i.e., the standard deviation) needs to be lower than the external interaction being measured. The control scheme described here, as well as the improved stability, should place us in the regime where these other critical issues can be addressed.

Acknowledgements

We would like to thank Edward Mulhern of the National Institute of Standards and Technology Mass and Force Group in the mechanical design and setup of the proof-of-concept system.

References

[1] Jabbour, Z. J., and Yaniv, S. L., 2001. "The kilogram and measurements of mass and force". *Journal of Research of the National Institute of Standards and Technology,* **106**(1), p. 25.

[2] Dushman, S., Lafferty, J. M., Brown, S. C., et al., 1962. "Scientific foundations of vacuum technique". *American Journal of Physics,* **30**(8), pp. 612–612.

[3] Nater, R., Reichmuth, A., Schwartz, R., Borys, M., and Zervos, P., 2009. *Dictionary of Weighing Terms*. Springer.

[4] Picard, A., Davis, R., Gläser, M., and Fujii, K., 2008. "Revised formula for the density of moist air (cipm-2007)". *Metrologia,* **45**(2), p. 149.

[5] Newell, D. B., 2014. "A more fundamental international system of units". *Physics Today,* **67**(7), pp. 35–41.

[6] Mulhern, E., and Stambaugh, C., 2017. "Characterization of the nist magnetic suspension mass comparator facility". *NCSLI Measure*.

[7] Mizushima, S., Ueda, K., Ooiwa, A., and Fujii, K., 2015. "Determination of the amount of physical adsorption of water vapour on platinum–iridium surfaces". *Metrologia,* **52**(4), p. 522.

[8] Davidson, S., Berry, J., Abbott, P., Marti, K., Green, R., Malengo, A., and Nielsen, L., 2016. "Air–vacuum transfer; establishing traceability to the new kilogram". *Metrologia,* **53**(5), p. A95.

[9] Davidson, S., 2010. "Determination of the effect of transfer between vacuum and air on mass standards of platinum–iridium and stainless steel". *Metrologia,* **47**(4), p. 487.

[10] Jabbour, Z., Abbott, P. J., Liu, R., and Williams, E., 2009. "A magnetic levitation technique for the simultaneous comparison of mass artifacts in air and vacuum". *IEEE Transactions on Instrumentation and Measurement,* **58**(4), pp. 878–883.

[11] Benck, E. C., Stambaugh, C., Mulhern, E., Abbott, P., and Kubarych, Z., 2017. "Progress on vacuum-to-air mass calibration system using magnetic suspension to disseminate the planck-constant realized kilogram". *ACTA IMEKO,* **6**(2), pp. 70–74.

[12] Stambaugh, C., and Mulhern, E., 2017. "An FEM analysis of the magnetic felds in the magnetic suspension mass comparator at nist". *NCSLI Measure*.

[13] Beams, J. W., Hulburt, C., Lotz Jr, W., and Montague Jr, R., 1955. "Magnetic suspension balance". *Review of Scientific Instruments,* **26**(12), pp. 1181–1185.

[14] Haynes, W. M., and Stewart, J. W., 1971. "A magnetic densimeter for low temperatures and high pressures". *Review of Scientific Instruments,* **42**(8), pp. 1142–1150.

[15] Masui, R., Haynes, W. M., Chang, R. F., Davis, H. A., and Sengers, J. M. H. L., 1984. "Densimetry in compressed fluids by combining hydrostatic weighing and magnetic levitation". *Review of Scientific Instruments,* **55**(7), pp. 1132–1142.

[16] Fujii, K., 2004. "Present state of the solid and liquid density standards". *Metrologia,* **41**(2), p. S1.

[17] Wagner, W., and Kleinrahm, R., 2004. "Densimeters for very accurate density measurements of fluids over large ranges of temperature, pressure, and density". *Metrologia,* **41**(2), p. S24.

[18] McLinden, M. O., Kleinrahm, R., and Wagner, W., 2007. "Force transmission errors in magnetic suspension densimeters". *International Journal of Thermophysics,* **28**(2), pp. 429–448.

[19] Schoonover, R. M., 1982. "A look at the electronic analytical balance". *Analytical Chemistry,* **54**(8), pp. 973A–980A.

[20] Clark, J. W., 1947. "An electronic analytical balance". *Review of Scientific Instruments,* **18**(12), pp. 915–918.

[21] Beams, J., 1950. "Magnetic suspension balance". *Physical Review,* **78**(4), p. 471.

[22] Gu, J., Kim, W.-j., and Verma, S., 2005. "Nanoscale motion control with a compact minimum-actuator magnetic levitator". *Journal of Dynamic Systems, Measurement, and Control,* **127**(3), pp. 433–442.

[23] Trumper, D. L., 1990. "Magnetic suspension techniques for precision motion control". PhD thesis, Massachusetts Institute of Technology.

[24] Kim, W.-J., and Trumper, D. L., 1998. "High-precision magnetic levitation stage for photolithography". *Precision Engineering,* **22**(2), pp. 66–77.

[25] Stambaugh, C., 2017. "The control system for the magnetic suspension comparator system for vacuum-to-air mass dissemination". *ACTA IMEKO,* **6**(2), pp. 75–79.

[26] MATLAB, 2016. *version R2016a*. The MathWorks Inc., Natick, Massachusetts.